

Transport of flexible chiral objects in a uniform shear flow

Peter Talkner, Gert-Ludwig Ingold, and Peter Hänggi

Institut für Physik, Universität Augsburg, Universitätsstraße 1, D-86135 Augsburg, Germany

E-mail: peter.talkner@physik.uni-augsburg.de

Abstract. The transport of slightly deformable chiral objects in a uniform shear flow is investigated. Depending on the equilibrium configuration one finds up to four different asymptotic states that can be distinguished by a lateral drift velocity of their center of mass, a rotational motion about the center of mass and deformations of the object. These deformations influence the magnitudes of the principal axes of the second moment tensor of the considered object and also modify a scalar index characterizing its chirality. Moreover, the deformations induced by the shear flow are essential for the phenomenon of dynamical symmetry breaking: Objects that are achiral under equilibrium conditions may dynamically acquire chirality and consequently experience a drift in the lateral direction.

PACS numbers: 83.50.-v, 05.60.Cd, 47.85.Np, 83.10.Pp

Submitted to: *New J. Phys.*

1. Introduction

The idea of achieving enantiomer separation on the basis of specific transport properties of chiral objects in flowing fluids [1, 2, 3] is very attractive because it opens the perspective to tackle this also industrially relevant task by purely physical means without the need of specific chemical agents.

Howard, Lightfoot and Hirschfelder [4] were the first to suggest the use of transport properties of asymmetric objects in order to separate differently crystallized enantiomers. Later, de Gennes discussed a mechanical way of separating chiral crystals [5]. Only recently, a lateral drift of screw-like objects in shear flows predicted by Brenner [6] was experimentally demonstrated for bodies with a linear extension of the order of centimeters [7], millimeters [8] and micrometers [9]. The direction of this drift, resulting from the coupling of the rotational and translational motion of a chiral object in a fluid, differs for objects with opposite chirality. The mutual interactions between flowing fluids and immersed chiral objects has been the subject of various recent experimental studies. The generation of flow patterns by actively rotating chiral objects was investigated in Ref. [10]. The control of actively moving nano-structured propellers was studied in Ref. [11]. In Ref. [12] the formation of chiral assemblies made of achiral components in a vortex flow is described.

Theoretical studies of the influence of the chirality of a macroscopic object on its transport properties were performed for sedimentation [13] and for shear flows [14]. Chiral planar three-atomic molecules were studied in clover leaf vortex flows [1] and in flows in channels of various geometries [15, 16]. In these two-dimensional studies fluctuating forces were taken into account in order to model the action of thermal fluctuations exerted on the molecules by the surrounding fluid. All studies [1, 13, 14, 15, 16] though are restricted to rigid objects.

Watari and Larson considered three-dimensional, four-atomic molecules which, in equilibrium, assume the form of a regular tetrahedron, which as such is achiral with respect to geometry [17]. When put into a shear flow these molecules are distorted in an asymmetric way due to differently deformable bonds between the atoms. As a consequence these molecules experience a lateral drift.

In the present work we study the motion of four-atomic molecules with *different* equilibrium bond-lengths but identical bond-strengths, see in eq. (2) below, being suspended in a uniform shear flow. The main mechanisms leading to a lateral drift of the molecules, i.e. to a motion perpendicular to the flow direction and to the direction in which the flow speed changes, can be summarized as follows. The shear field of the flow leads to a rotation of the molecule which then, like a small propeller, moves in, or opposite to the direction of the vorticity of the flow. We demonstrate that the rotation is essentially determined by the advection of the atoms with the fluid motion and only little influenced by hydrodynamic interactions between the atoms. In a uniform shear flow a coupling between rotational and translational motion, however, only is possible due to hydrodynamic interactions between the atoms.

As for the motion of molecular motors [2], the direction of the lateral drift is difficult to predict. In general it depends on all parameters of the system and also on the initial conditions with which the molecule is started. These initial conditions may belong to different domains of attraction, eventually leading to different attractors, which may display different forms of rotation of the molecule, and consequently different drift behaviors, even with opposite signs.

Due to the deformability of the considered molecules, chiral attractors may exist for molecules with achiral equilibrium configurations and consequently also achiral molecules may experience a lateral drift displaying a dynamical symmetry breaking. The lateral drift, however, vanishes on average because for a molecule with achiral equilibrium configuration chiral attractors can only come in mutually mirror symmetric pairs.

The paper is organized as follows. In Section 2 we introduce a class of “spiral” molecules, the geometry of which is described by only three parameters, and specify their equations of motion in terms of bond strengths and hydrodynamic interactions. Further, we introduce the most important quantities needed for the analysis of the numerical solutions of the equations of motion (Section 2.2). In Section 3 we present the results concerning the center of mass motion (Section 3.1), the rotational motion (Section 3.2) and the internal motion (Section 3.3) with particular emphasis on the dynamical symmetry breaking (Section 3.3.1). The role of hydrodynamic interactions is discussed in Section 4. The paper closes with a summary and an outlook in Section 5.

2. The model

2.1. Spiral molecules and equation of motion

In the present case study we consider “molecules” consisting of four identical “atoms” modeled by spheres of radius a . The equilibrium configuration of a free molecule, i.e. a stable configuration with balanced bonding forces between the atoms, is assumed to be of helical form. This form is constructed by positioning the centers of the spheres on a cylinder mantle of radius ρ . Given the location of the first atom, \mathbf{R}_1 , the next one, \mathbf{R}_2 , is found upon rotation by an angle φ about the cylinder axis combined with a translation by h parallel to the cylinder axis, and so on with the third and fourth atom, yielding the respective positions \mathbf{R}_3 and \mathbf{R}_4 . Hence, if the cylinder axis coincides with the z -direction of a coordinate system and the first atom lies on the x -axis of the coordinate system, then the following vectors point to the centers of the atoms sitting on a spiral:

$$\mathbf{R}_n = \rho \mathbf{e}_x \cos[(n-1)\varphi] + \rho \mathbf{e}_y \sin[(n-1)\varphi] + h(n-1)\mathbf{e}_z, \quad n = 1, 2, 3, 4. \quad (1)$$

We model the bonding forces between the atoms of such a “spiral” molecule by nonlinear, so-called FENE-Fraenkel (Finitely Extensible Nonlinear Elastic) springs [18]. If \mathbf{r} is the vector connecting two atoms, then the force acting between these atoms is

given by

$$\mathbf{f} = k(r-l) \frac{(r_+ - l)(l - r_-)}{(r_+ - r)(r - r_-)} \frac{\mathbf{r}}{r}, \quad \text{for } r_- < r < r_+, \quad (2)$$

where $r = |\mathbf{r}|$ is the distance between the atoms, l the equilibrium length of the spring, k the spring-constant describing the Hookean behavior of the spring for small extensions about the equilibrium length, and $s < 1$ is a nonlinearity parameter of the spring. At the extensions

$$r_{\pm} = (1 \pm s)l \quad (3)$$

the force diverges so that the bond-length between two atoms is restricted to the indicated, finite range.

In contrast to Ref. [17], we choose *identical* force parameters k and s for the bonds, only the equilibrium bond lengths l may differ. Hence, a possible chirality of the equilibrium configuration of a molecule is solely determined by its geometry: According to the standard definition, a molecular configuration is *achiral* if a movement of the molecule, i.e. a combination of translations and rotations in three-dimensional space, exists such that it matches its mirror image; in any other case the configuration is *chiral*.

When the molecule is suspended in a flowing fluid, advective forces act on the individual atoms, which in addition mutually influence their motions by hydrodynamic interactions. The total action of the fluid on the atoms will be described by a mobility tensor $\mathbf{H}_{n,m}$ relating the forces acting on the m th particle to the velocity of the n th particle. The deterministic, overdamped motion of the molecule in a fluid flow with the velocity field $\mathbf{v}(\mathbf{r})$ is then given by

$$\dot{\mathbf{r}}_n = \mathbf{v}(\mathbf{r}_n) + \sum_{m=1}^4 \mathbf{H}_{n,m} \cdot \mathbf{f}_m, \quad (4)$$

where \mathbf{f}_m is the total force acting on the m th atom, i.e. the sum of the FENE-Fraenkel forces (2) exerted by the other three atoms, and the dot denotes differentiation with respect to time. For sufficiently small spheres representing the atoms, inertial terms can be neglected [19]. We shall describe the mobility by the Rotne-Prager tensor which includes the hydrodynamical interactions up to second order in the ratio $a/r_{n,m}$ of the atomic radius a and the distance $r_{n,m}$ between the n th and the m th atom. It is given by [20]

$$\mathbf{H}_{n,m} = \frac{1}{6\pi\eta a} \left[\delta_{n,m} \mathbb{1} + (1 - \delta_{n,m}) \frac{3a}{4r_{n,m}} \mathcal{H}_{n,m} \right], \quad (5)$$

with

$$\mathcal{H}_{n,m} = \begin{cases} \left(1 + \frac{2a^2}{3r_{n,m}^2}\right) \mathbb{1} + \left(1 - \frac{2a^2}{r_{n,m}^2}\right) \frac{\mathbf{r}_{n,m}\mathbf{r}_{n,m}}{r_{n,m}^2} & \text{for } r_{n,m} \geq 2a \\ \left(1 - \frac{9r_{n,m}}{32a}\right) \mathbb{1} + \frac{3\mathbf{r}_{n,m}\mathbf{r}_{n,m}}{32ar_{n,m}} & \text{for } r_{n,m} < 2a \end{cases}, \quad (6)$$

where $\mathbb{1}$ denotes the unit tensor in the three-dimensional space, η the viscosity of the fluid, and $\mathbf{r}_{n,m} = \mathbf{r}_m - \mathbf{r}_n$ the vector pointing from the position of the n th to that of the m th atom.

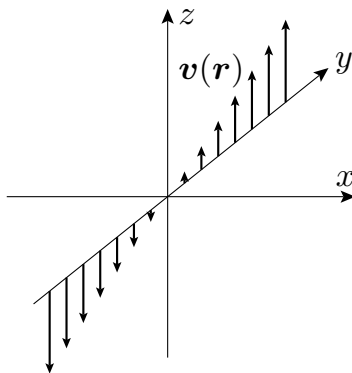


Figure 1. Uniform shear flow: The velocity is independent of x , points in z direction, and varies its magnitude proportionally to y .

In passing we mention that thermal noise leads to additional random contributions in the equations of motion, see Ref. [21], yielding

$$\dot{\mathbf{r}}_n = \mathbf{v}(\mathbf{r}_n) + \sum_{m=1}^4 \mathbf{H}_{n,m} \mathbf{f}_m + 2k_B T \sum \boldsymbol{\sigma}_{n,m} \cdot \boldsymbol{\xi}_m(t), \quad (7)$$

where $\boldsymbol{\xi}_n(t)$ are mutually independent three-dimensional Gaussian, white noise vectors, satisfying

$$\langle \boldsymbol{\xi}_n(t) \boldsymbol{\xi}_m(s) \rangle = \delta_{n,m} \mathbb{1} \delta(t-s). \quad (8)$$

The fluctuation-dissipation theorem requires that the coupling to the noise, $\boldsymbol{\sigma}_{i,j}$, is related to the Rotne-Prager tensor according to

$$\mathbf{H}_{n,m} = \sum_{k=1}^4 \boldsymbol{\sigma}_{n,k} \cdot \boldsymbol{\sigma}_{j,m}. \quad (9)$$

In the present work though we neglect all influences stemming from thermal noise, and, hence restrict ourselves to the discussion of the deterministic equations of motion in (4). We shall consider a uniform shear flow given by

$$v_x = v_y = 0, \quad v_z = \kappa y. \quad (10)$$

where κ denotes the shear rate, see Figure 1. Even in this seemingly simple case the deterministic equations of motion can only be solved by numerical means. For that purpose we employed a LSODA code of variable order and step-length [22, 23] as available from the open source SciPy package [24].

In the numerical treatment we used dimensionless variables where lengths are measured in units of the atomic radius a and times in units of the inverse shear rate κ^{-1} . Apart from six parameters which fix the equilibrium geometry of a molecule consisting of four atoms in general, or three in the present case of a spiral molecule as defined by eq. (1), two further parameters are needed for the characterization of the forces. As

such we will choose the nonlinearity parameter s and the dimensionless spring constant $k_f = k/(6\pi\eta a^2\kappa)$. With this choice the deterministic equations of motion read

$$\dot{\mathbf{x}}_n = \mathcal{S}\mathbf{x}_n + k_f \sum_{m=1}^4 \mathcal{H}_{n,m} \cdot \mathbf{F}_m, \quad (11)$$

where \mathcal{S} is the shear tensor, which has vanishing matrix elements apart from the z - y element, being unity, and \mathbf{F}_m denotes the dimensionless force exerted on the j -th particle by the adjacent particles, reading

$$\mathbf{F}_m = \sum_{n \neq m} \frac{x_{n,m} - \ell_{n,m}}{1 - (1 - x_{n,m}/\ell_{n,m})^2} \frac{\mathbf{x}_{n,m}}{x_{n,m}} \quad (12)$$

for $(1 - s)\ell_{n,m} < x_{n,m} < (1 + s)\ell_{n,m}$.

Here $\mathbf{x}_n = \mathbf{r}_n/a$, $\mathbf{x}_{n,m} = \mathbf{x}_n - \mathbf{x}_m$, $x_{n,m} = |\mathbf{x}_{n,m}|$ and $\ell_{n,m} = |\mathbf{R}_n - \mathbf{R}_m|/a$ denote the dimensionless positions, distance vectors, the actual distances and the equilibrium distances between atoms n and m , respectively.

Possible initial conditions for the integration of the equation of motion (11) are given by any set of atomic positions that obey the restrictions imposed by the FENE-Fraenkel forces (13). Here we confine ourselves to equilibrium configurations of the free molecules. For further details of how the orientations are chosen, see Sect. 3.

2.2. Characteristics of the mechanical molecular states

In the framework of the overdamped dynamics of eq. (11) the mechanical state of the molecule is uniquely described by the positions $\mathbf{x}_n(t)$ of the four atoms. A reduced description is provided by the center of mass of the molecule consisting of four atoms of equal mass, consequently reading

$$\mathbf{X} = \frac{1}{4} \sum_n \mathbf{x}_n. \quad (13)$$

The spatial orientation of the molecule can conveniently be characterized by the three principal axes of the symmetric tensor of second moments of the atomic positions, \mathbf{M} , defined by its elements

$$M_{i,j} = \frac{1}{4} \sum_n (x_i^n - X_i)(x_j^n - X_j), \quad (14)$$

where x_i^n denotes the i -th Cartesian position component of the n -th atom. The orientations of the principal axes are determined by the normalized eigenvectors \mathbf{u}_i and their magnitudes by the corresponding eigenvalues λ_i of the tensor of second moments. Hence, they result from the eigenvalue problem

$$\mathbf{M}\mathbf{u}_i = \lambda_i\mathbf{u}_i, \quad (15)$$

where $\mathbf{M} = (M_{i,j})$.

The velocity vector $\boldsymbol{\omega}$ of the instantaneous rotation of the molecule in the frame co-moving with the molecule's center of mass is determined by the orientation and velocity

of any body-fixed tripod. Here we use the principal axes of the second moments to obtain

$$\boldsymbol{\omega} = -\frac{1}{2} \sum_i \dot{\mathbf{u}}_i \times \mathbf{u}_i, \quad (16)$$

where the dot denotes a derivative with respect to time and $\mathbf{u} \times \mathbf{v}$ the vector product of the vectors \mathbf{u} and \mathbf{v} . By means of the eigenvalue equation (15) one may express $\dot{\mathbf{u}}_i$ in terms of the time derivative of \mathbf{M} , to yield

$$\boldsymbol{\omega} = \frac{1}{2} \sum_{i \neq j} \frac{\mathbf{u}_j \cdot \dot{\mathbf{M}} \mathbf{u}_i}{\lambda_j - \lambda_i} \mathbf{u}_j \times \mathbf{u}_i, \quad (17)$$

where $\mathbf{u} \cdot \mathbf{v}$ denotes the scalar product of the vectors \mathbf{u} and \mathbf{v} .

As a measure of the deformation of a molecule we consider the ratio of volumes taken in the distorted state and the equilibrium shape. As molecular volume one may assign the square root of the product of the magnitudes of the principal axes, i.e.,

$$V = (\lambda_1 \lambda_2 \lambda_3)^{1/2}. \quad (18)$$

Whether a molecule is chiral cannot be decided on the basis of its second moments of positions. For this purpose, we use the isotropic chirality index G_0 , which is invariant under translations and rotations of the molecule [25], in its dilation invariant form. For a molecule consisting of four atoms of equal mass and size it becomes

$$G_0 = \frac{1}{3} \sum_{i,j,k,l} \frac{\mathbf{x}_{i,j} \cdot (\mathbf{x}_{k,l} \times \mathbf{x}_{i,l}) (\mathbf{x}_{i,j} \cdot \mathbf{x}_{j,k}) (\mathbf{x}_{j,k} \cdot \mathbf{x}_{k,l})}{(x_{i,j} x_{j,k} x_{k,l})^2 x_{i,l}}. \quad (19)$$

The sum is extended over all sets i, j, k, l , taken from the permutations of $\{1, 2, 3, 4\}$. This index has the general property that it assumes the same absolute value but opposite signs for enantiomers, i.e. pairs of configurations that are mirror images of each other. Hence, achiral configurations have a vanishing chirality index.

For a spiral molecule, the chirality index is a function of the relative rise ρ/h and the screw angle φ . It is an antisymmetric function about the line $\varphi = \pi$, see Fig. 2(a), and possesses a singularity at $\varphi = 2\pi/3$ and $h/\rho = 0$. Along the lines $h/\rho \approx -(\varphi - 2\pi/3)$ for $\varphi < 2\pi/3$, and $h/\rho \approx 0.95(\varphi - 2\pi/3)$ for $\varphi > 2\pi/3$, the chirality index forms a ridge and a valley, respectively. Approaching the singularity along the ridge, the chirality index converges to the approximate value 0.289 while it approaches the opposite value -0.289 along the bottom of the valley.

Since all configurations with $h/\rho = 0$ are planar, and, hence achiral, the chirality index exactly vanishes on the line $h/\rho = 0$. In the remaining part of the φ - h/ρ -plane the chirality index has three extrema on each side of the symmetry line $\varphi = \pi$. Local extrema are located at $\varphi \approx 0.8908\pi$, $h/\rho \approx 0.2073$ and $\varphi \approx 0.9291\pi$, $h/\rho \approx 0.584$. The absolute maximum is at $\varphi \approx 0.656\pi$, $h/\rho \approx 2.516$, see Fig. 2(a). The chirality index vanishes on the solid and dashed curves in Fig. 2(b). These curves result from constraints on the bond lengths (see Appendix). Along the dashed curve emerging from $\varphi = \pi/2$, $h/\rho = 0$, and ending in $\varphi = \pi$, $h/\rho = 0$, the configurations possess a group of four and another one of two equally long edges, see Fig. 3(b). Since the corresponding

configurations possess a symmetry plane, they are achiral. The faces of these tetrahedra are made of identical isosceles triangles. Also the configurations on the curve starting at $\varphi = 2\pi/3$, $h/\rho = 0$ and reaching $\varphi = \pi$, $h/\rho = 2/\sqrt{3}$ are achiral; the faces of these configurations consist in two identical equilateral and two identical isosceles triangles; consequently five of the six edges have the same length, see Fig. 3(c). The analytic forms of the achiral curves are derived in the Appendix. Examples of different types of configurations are displayed in Fig. 3. There exists a third node line of G_0 which, however, does not correspond to achiral configurations. We could not find an analytic expression for this line which emerges from $\varphi \approx 0.46\pi$, $h/\rho = 0$ and ends in $\varphi \approx 0.88\pi$, $h/\rho = 0$. The three node lines of the chirality index meet in a single point which corresponds to a regular tetrahedron. For the fact that a vanishing value of the chirality index does not necessarily correspond to an achiral configuration, see in Ref. [26].

3. Results

For our investigations, we selected spiral molecule configurations on four cuts in the parameter plane displayed in Fig. 2(a). Three of these cuts (A, B, C) are taken at constant relative rise $h/\rho = 0.2073, 0.584$, and 2.5162 , respectively, each one for $\varphi \in (0, \pi)$. For the two smaller values of h/ρ we chose a relatively large radius $\rho = 7$ in order to avoid any collision of the atoms within a molecule, and the smaller radius $\rho = 2$ for the large relative rise. The vertical cut D is determined by the screw angle $\varphi = 2\pi/3$, radius $\rho = 3$ and relative rise $h/\rho \in (0, 5)$.

As initial configurations we took the equilibrium configurations according to eq. (1), rigidly translated such that the center of mass falls into the origin. Finally, rigid rotations of the molecule about its center of mass were performed. Between 500 and 5000 rotations were sampled from the uniform distribution on the three-dimensional rotation group [27], i.e. from the Haar measure of $SO(3)$. We typically let run each trajectory for 4000 time units [κ^{-1}]. In the majority of the cases the trajectories have relaxed toward a stationary regime long before the time span of 4000. In this state the center of mass acquires a finite velocity in z -direction, depending on the precise initial position of the molecule, and the y -component of the velocity may perform small oscillations but vanishes on average. The lateral motion in the direction of the vorticity coinciding with the x -direction in the present case is characterized by an average velocity superimposed by bounded modulations which were always periodic. Fig. 4 displays the components of the center of mass for the same molecule and its mirror image in four different asymptotic motional states.

3.1. Center of mass motion

The fact that the x -component of the center of mass moves at a finite average velocity is apparently related to the chirality of the considered molecule: For any achiral molecule in the considered shear flow the opposite x -directions are equivalent. This symmetry is

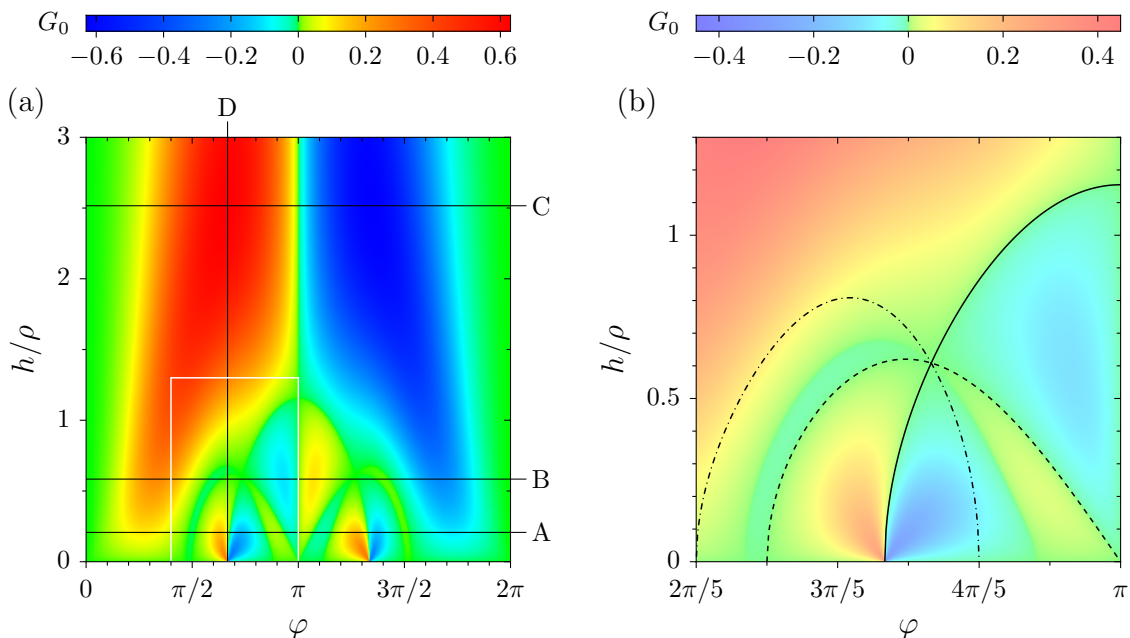


Figure 2. The chirality index G_0 defined in eq. (19) is displayed for spiral molecules as a function of the screw angle φ and the relative rise h/ρ , see eq. (1). On the panel (a) the symmetry $G_0 \rightarrow -G_0$ upon a reflection on the line $\varphi = \pi$ is clearly visible. The four black lines labeled by A – D indicate four cuts through the parameter plane, see the text in Section 3 as well as Fig. 5 below. The lines A and B are defined by local maxima of the chirality index. On C and D the absolute maximum of G_0 is located. The panel (b) represents a blow-up of the region marked in the panel (a) by the white lines. Note that for the purpose of better visibility different color scales are used in the two panels. The black lines in (b) indicate those curves on which two of the three edge lengths $l(k)$, $k = 1, 2, 3$ between atoms with positions \mathbf{R}_n and \mathbf{R}_{n+k} are equal, see the Appendix. The solid line represents achiral configurations with $l(1) = l(2)$ which have five equally long edges. It starts at the singularity of G_0 at $\varphi = 2\pi/3$ and $h/\rho = 0$ and ends at $\varphi = 4\pi/3$ and $h/\rho = 0$. Along the dashed line $l(1) = l(3)$ holds. These configurations have two and four equally long edges and are also achiral. On the dashed-dotted line, where $l(2) = l(3)$, the configurations possess two triples of equally long edges, and the chirality index is non-zero everywhere except at the points with $h/\rho = 0$ and at the crossing point of the three lines which corresponds to a regular tetrahedron. Note that there is still a third curve recognizable by the green color on which the chirality index vanishes in spite of the chirality of the corresponding configurations.

broken by the presence of a chiral molecule and, according to the Curie principle [29], the molecule will perform a directed motion in either of the two directions. This argument is further corroborated if one launches the chiral partner of a considered molecule into the shear flow with initial atomic positions obtained from the original ones by mirroring on the y - z plane. Then one indeed finds the molecule moving in the opposite x -direction as illustrated by the panel pairs ((a),(ma)), ((b),(mb)), etc. in Fig. 4 displaying the corresponding pairs of mirror images.

Inserting a molecule into the shear flow with randomly chosen orientations as

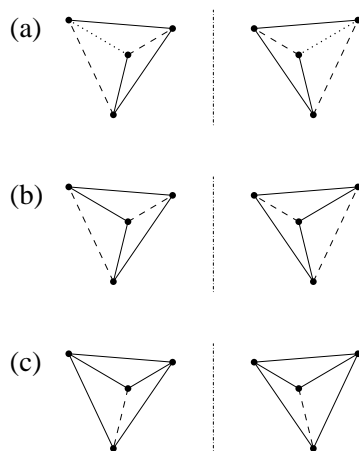


Figure 3. Panel (a) illustrates a generic spiral molecule with three and two edges of equal lengths and a sixth edge of different length. The edges of equal lengths are drawn correspondingly. Panel (b) presents a configuration on the dashed curve displayed in Fig. 2(b) with two and four equally long edges while the configuration in panel (c) has five equally long edges representing a configuration on the solid curve depicted in Fig. 2(b). The right part of the figure represents the corresponding mirror images. The cases (b) and (c) are achiral.

described above, one typically finds between one and four different motional states of the center of mass, which are asymptotically reached at large times. We determined the corresponding average velocities $\langle v_x \rangle$ by a least-square fit of the x -components of the center of mass to a uniform motion, yielding

$$\langle v_x \rangle = \frac{12}{N(N+1)(N+2)\tau} \sum_{n=0}^N \left(n - \frac{N}{2}\right) X_x(t_0 + n\tau). \quad (20)$$

In most cases we used $t_0 = 3000$, $N = 1000$ and $\tau = 1$. Since the different motional states typically are distinguished by their average velocities, these velocities may be used to roughly classify the asymptotic states as exemplified in Fig. 5. A precise classification would require the additional knowledge of the molecule's orientation and six bond lengths and hence would be difficult to visualize.

In addition to the average center of mass velocity the behavior of the chirality index G_0 of the initial configuration is depicted as red line in Fig. 5 along the respective cuts. This index correlates with the average velocities at best in a qualitative way. Of particular interest here is the behavior of the average velocity in the vicinities of the zeroes of the chirality index as a function of the screw angle φ indicated by the blue lines.

As mentioned at the end of Section 2, one has to distinguish between chiral and achiral zeroes of the chirality index G_0 . Indeed, close to chiral zeroes, none of the there existing velocity branches does cross the zero line. But also near the achiral zeroes, branches with finite velocities may exist. They may coexist with a branch with vanishing average velocity, which, however, may also be missing. The $x \leftrightarrow -x$ -inversion

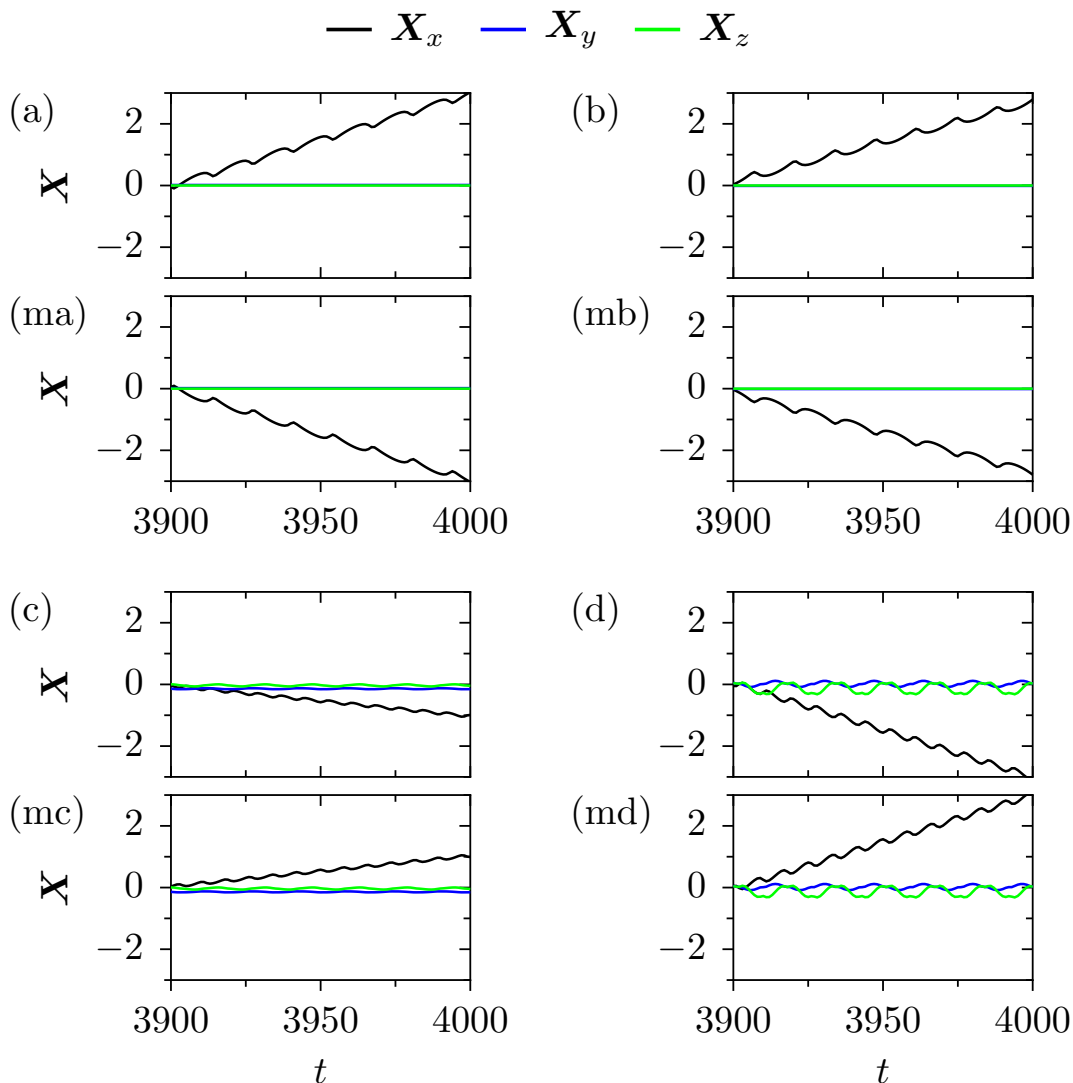


Figure 4. The center of mass motion of a spiral molecule with an equilibrium configuration on cut A specified by $h/\rho = 0.2073$, $\rho = 7$ and $\varphi = 0.87\pi$ asymptotically reaches one of the four different states depicted in the panels (a), (b), (c), (d) depending on the initial orientation of the molecule. If this orientation is randomly drawn from a uniform distribution, then one finds the cases (a) with a probability of 0.19, (b) with 0.22, (c) with 0.50, and (d) with 0.09. The x -component of the center of mass is displayed in black. It is shifted by its actual value taken at the time $t=3900$; the y -component, which is either constant, or periodically oscillating is depicted by the blue line; from the z -component (green) an average uniform motion is subtracted. The configurations mirrored at the y - z -plane starting from the corresponding mirror images of the initial orientations of (a)-(d) result in the motion patterns displayed in the panels (ma)-(md), which obviously coincide with the mirror images of panels (a)-(d). The average velocities $\langle v_x \rangle$ in x -direction, see eq. (20) below, in the cases (a) and (ma) are ± 0.02974 ; correspondingly one finds $\langle v_x \rangle = \pm 0.02594$ in (b) and (mb), $\langle v_x \rangle = \mp 0.00994$ in (c) and (mc), and $\langle v_x \rangle = \mp 0.03044$ in (d) and (md). In all cases the mirrored patterns occur with the probabilities of the corresponding original ones as specified above.

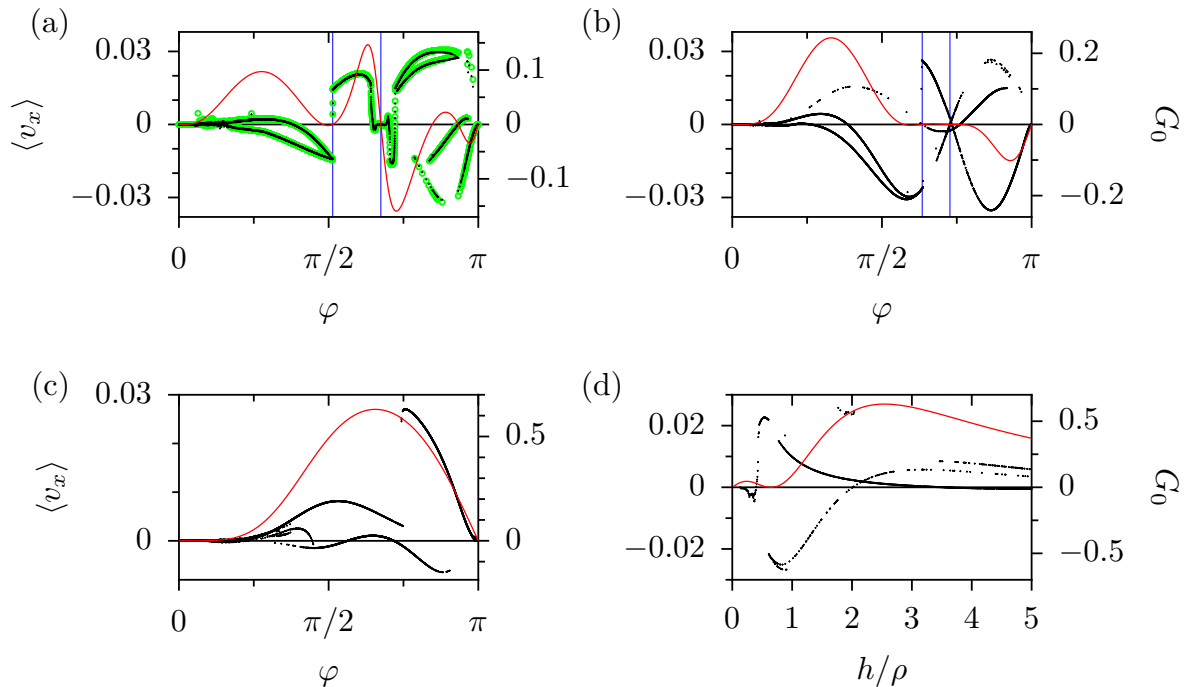


Figure 5. Asymptotic average velocities $\langle v_x \rangle$ were estimated for molecules with equilibrium configurations along the four cuts A – D in the φ - h/ρ parameter plane displayed in Fig. 2(a). The initial conditions were randomly oriented according to the uniform measure on the three-dimensional rotation group. Panels (a), (b) and (c) correspond to the horizontal cuts A, B, C, along $h/\rho = 0.2073$ with $\rho = 7$, $h/\rho = 0.584$ with $\rho = 7$, as well as $h/\rho = 2.5162$ with $\rho = 3$, respectively. Panel (d) represents the vertical cut D for $\varphi = 2\pi/3$, $\rho = 5$, and $h/\rho \in (0, 5)$. For comparison, the chirality index G_0 defined in eq. (19) is indicated as a red line with the corresponding scale at the right-hand side ordinate. The vertical blue lines in panels (a) and (b) mark the respective values of the screw angles at which the equilibrium configurations are achiral. In all panels the black dots represent the result of the solution of the equations of motion (11) with the full Rotne-Prager tensor (6). The average velocities group into up to four well defined branches at most parameter values. In panel (a), additionally the numerical results obtained from eq. (11) with the Oseen tensor (25) are displayed as small green circles. The overall agreement of the two approaches is very good, see also Section 4.

symmetry though is restored on average since there are always pairs of branches with opposite velocities which are populated with equal probability. As we shall discuss in more detail below, the branches with finite average velocities at achiral zeroes of the chirality index represent states of dynamically broken symmetry.

3.2. Rotational motion

In the asymptotic state, when the center of mass undergoes a periodically modulated uniform motion, the instantaneous rotation axis predominantly points into the x -direction, possibly superimposed by small, oscillatory deviations orthogonal to this

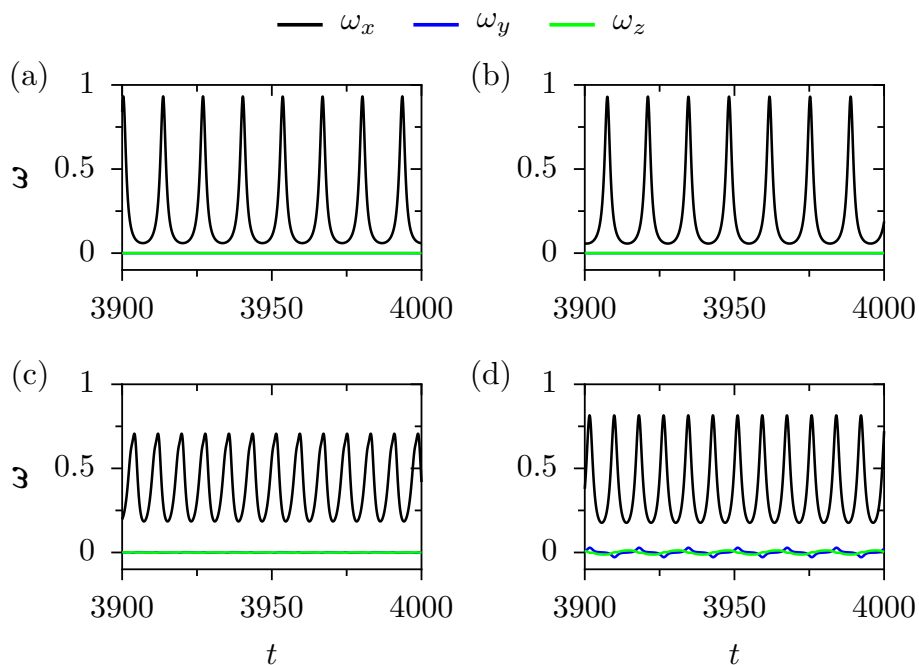


Figure 6. The components of the instantaneous axis of rotation, ω , for the configuration with $\varphi = 0.87\pi$, $h/\rho = 0.2073$ and $\rho = 7$ corresponding to the maximum of G_0 on cut A. The component ω_x pointing in the vorticity direction of the shear flow is marked in black, the y - and z -components in blue and green, respectively. Panels are labeled as in Fig. 4. In all cases the rotation about the vorticity direction is dominant. Only in panel (d) a slight tumbling of the axis is noticeable.

direction. Fig. 6 depicts the components of the instantaneous rotation axis for different asymptotic motional states of the same molecule. This orientation of the instantaneous rotation axis appears as a rather natural consequence of the considered flow geometry with uniform vorticity pointing into the x -direction. A conspicuous tumbling behavior of the instantaneous rotation axis was found in a case of dynamically broken symmetry, see Fig 12a. The rotation speed undergoes pronounced oscillations in the majority of cases. In the asymptotic states in which the instantaneous rotation axis points in the x -direction the molecule is typically found to be oriented such that one of its principal axes is aligned with the direction of rotation. The transient behavior and the approach to the specific asymptotic states of the angles enclosed by the principal axes and the instantaneous rotation axis is exemplified in Fig. 7.

Due to the lack of any symmetry plane in a chiral molecule, there are two possible ways to orient a principal axis along the instantaneous axis of rotation. However, we found different velocity branches corresponding to opposite orientations only for alignments of the rotation axis with the middle principal axis, and only if the skewness S_ω of the molecule along the axis of rotation vanishes within numerical precision. As a measure for the skewness of a molecule relative to the vector of angular velocity ω we take the third root of the third moment of the atomic positions \mathbf{x}_n relative to the center

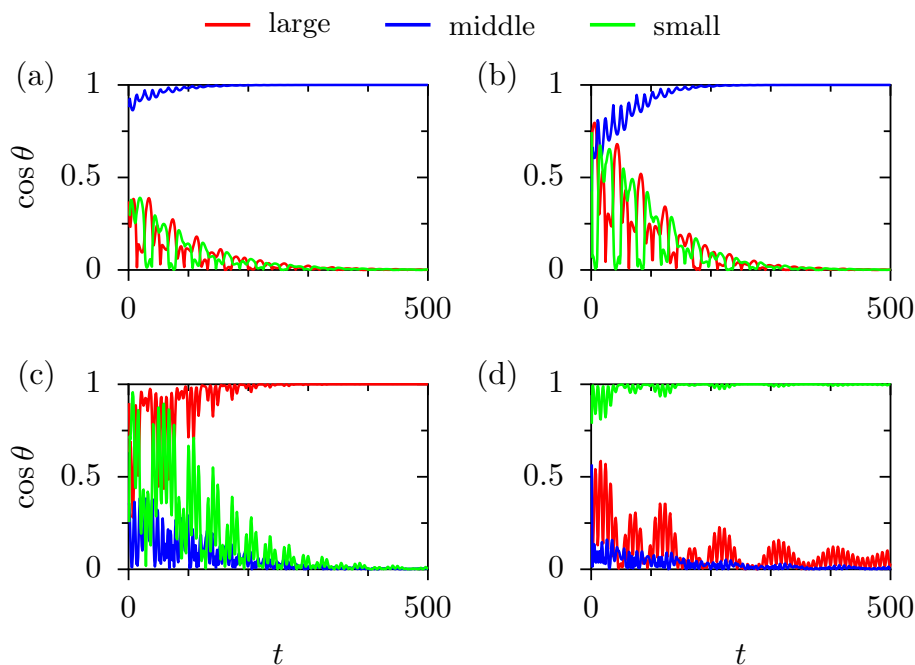


Figure 7. The time evolution of the cosines of the angles between the instantaneous vector of rotation and the eigenvectors of the second moments of positions, $\cos \theta_i = \boldsymbol{\omega} \cdot \mathbf{u}_i / |\boldsymbol{\omega}|$, for the configuration with $\varphi = 0.87\pi$, $h/\rho = 0.2073$ and $\rho = 7$ is depicted for different initial orientations. The asymptotic motion of the center of mass as well as the motion of the axes of instantaneous rotations are displayed in Figs. 4 and 6, respectively, with the panels labeled consistently. The cosine of the eigenvector corresponding to the largest eigenvalue is red, to the middle one blue and to the smallest one green. In panels (a) and (b) the middle principal axis asymptotically aligns with the rotation axis, while the initial orientations in panels (c) and (d) lead to alignments with the largest and the shortest axis, respectively.

of mass projected onto the direction of the rotation axis, $\mathbf{e}_\omega = \boldsymbol{\omega}/|\boldsymbol{\omega}|$, hence, reading

$$S_\omega = \left(\sum_n \left((\mathbf{x}_n - \mathbf{X}) \cdot \mathbf{e}_\omega \right)^3 \right)^{1/3}. \quad (21)$$

The maximum number of branches we detected was four. For $\eta/\rho = 0.2073$, $\rho = 7$ and screw angles approximately ranging between $\varphi = 0.8\pi$ and $\varphi = 0.9\pi$ one observes single alignments to the small and the large axes and both orientations relative to the middle axis. Fig. 8 represents the time evolution of the skewness for a molecule with initial orientations belonging to different domains of attraction.

3.3. Internal motion and dynamical symmetry breaking

Also in the reference frame that moves with the center of mass and rotates with the instantaneous angular velocity, the molecules generally are not at rest but undergo internal motions characterized by changing bond lengths and bond angles. These distortions then lead to modulations of the magnitudes of the principal axes as

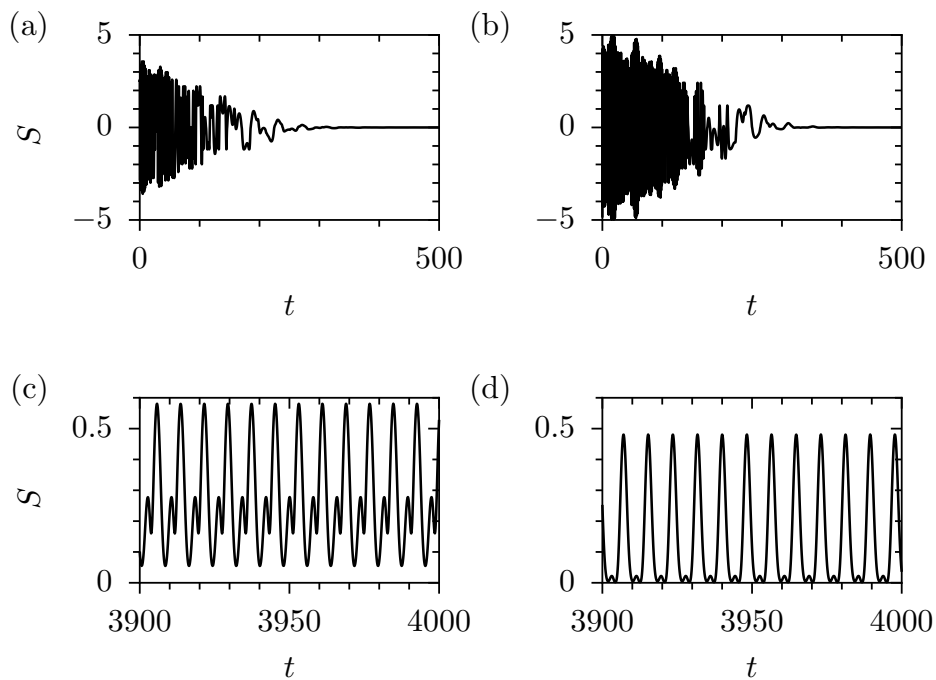


Figure 8. For those initial orientations of the configuration with $\varphi = 0.87\pi$ $h/\rho = 0.2073$ and $\rho = 7$ which finally approach two different states both rotating about the middle axis, see Fig. 7 (a), (b), the third moments of the positions projected onto the instantaneous axis of rotation, S_ω , defined in eq. (21), relax to zero. For other initial orientations the skewness S_ω asymptotically undergoes rotations, see panels (c) and (d).

exemplified in Fig. 9. The resulting periodic relative volume changes of the molecule are presented in Fig. 10.

3.3.1. Dynamical symmetry breaking In molecules with achiral equilibrium configurations, a deformation caused by shear forces in general will break its mirror symmetry and hence render the molecules chiral. This mechanism is at the heart of the effect of *dynamical symmetry breaking* that can be observed at achiral zeroes of the chirality index G_0 .

For spiral molecules the three-dimensional achiral configurations are found on two curves in the φ - h/ρ -parameter plane, reading

$$(h/\rho)_1 = \left[\frac{2}{3} (\cos(2\varphi) - \cos(\varphi)) \right]^{1/2}, \quad 2\pi/3 < \varphi < 4\pi/3, \quad (22)$$

$$(h/\rho)_2 = \frac{1}{2} [(\cos(3\varphi) - \cos(\varphi))]^{1/2}, \quad \pi/2 < \varphi < 3\pi/2. \quad (23)$$

For a derivation see the Appendix. The branch $(h/\rho)_1$ corresponds to the solid line and $(h/\rho)_2$ to the dashed line in the Fig. 2(b). Fig. 11(a) displays the asymptotic average velocities in x -direction and the corresponding average values of the chirality index for the achiral configuration at $\varphi = 0.7271607\pi$ and $\rho = 7$ on the curve $(h/\rho)_1$. As for all

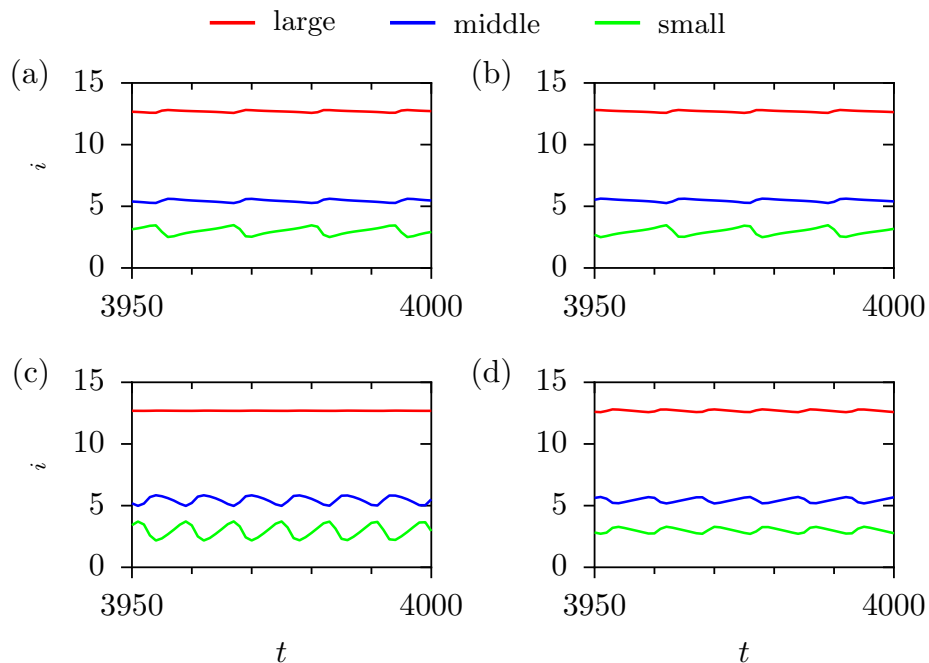


Figure 9. The magnitude of the principal axes of the second position moments for the configuration with $\varphi = 0.87\pi$, $h/\rho = 0.2073$ and $\rho = 7$. In the four different asymptotic states, which are labeled in the same way as in the previous Figures, the magnitudes of the principal axes undergo periodic modifications. In the two cases with positive asymptotic velocities, (a) and (b), these modifications are almost identical. Noticeable differences occur between the states characterized by rotations about the large and the short principal axes, displayed in panels (c) and (d), respectively.

achiral configurations on this curve, it possess five equally long edges. In the present case, the sixth edge is shorter than the others. This molecule is initially oriented in such a way that the symmetry plane containing both the short edge and the z -axis encloses an angle α with the y -axis, see the Fig 11(b). Depending on this angle α , two different pairs of asymptotic states with non-vanishing velocities and chiral indices of opposite signs are approached with time. The average chirality index was obtained as an algebraic mean over a time window of length 1000 in the asymptotic regime. Because a rotation about the z -axis by $\alpha = \pi$ leaves any of these initial configurations invariant the resulting pattern of average velocities and chiral indices is periodic with period π . The rotational motion and the orientation of the principal axes are presented in Fig. 12 for two of the chiral attractors of an achiral molecule.

The average asymptotic velocities on a part of the achiral curve $(h/\rho)_1$ given by eq. (22) were determined for $\rho = 5$. Similarly as on the other cuts, equilibrium configurations were determined from eq. (1) at 2001 equally spaced angular values for $\varphi \in [0.67\pi, \pi]$; subsequently their centers of mass were translated to the origin and randomly rotated about the center of mass. With these initial conditions the equations of motion were integrated up to $t = 8000$. The average velocity $\langle v_x \rangle$ was determined according to eq. (20) for $t_0 = 7000$, $N = 1000$ and $\tau = 1$. Fig. 13 presents

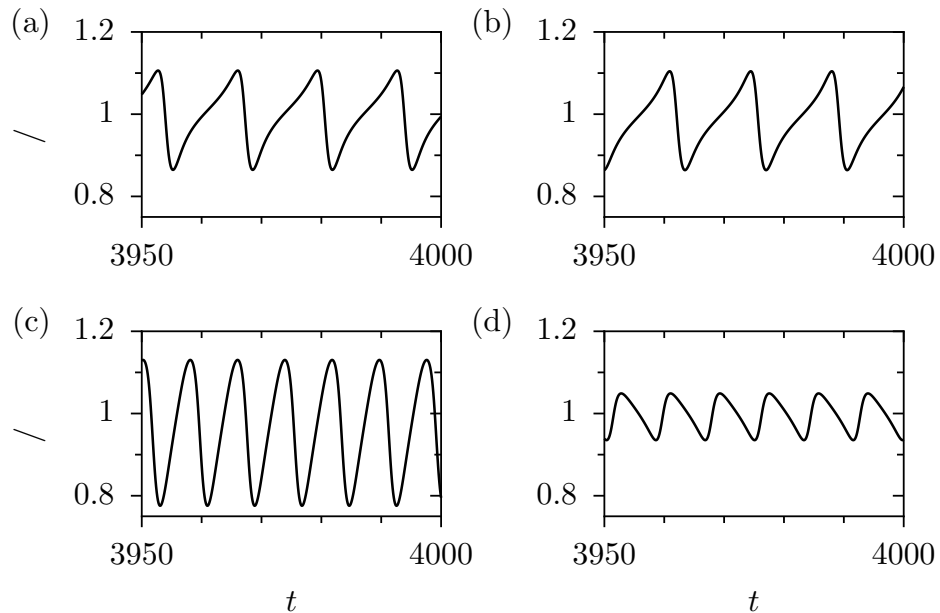


Figure 10. The ratio of the actual to the equilibrium volume for different initial orientations of the configuration with $\varphi = 0.87\pi$, $h/\rho = 0.2073$ and $\rho = 7$ in the same order as in Figs. 6 – 9. For the two asymptotic states (a) and (b) moving in the positive x -direction the volume variations are essentially identical but different from both states (c) and (d).

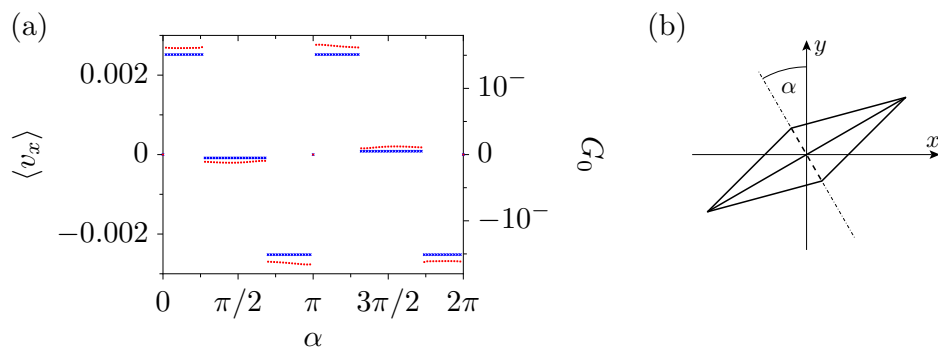


Figure 11. On the panel (a), different chiral-symmetry breaking attractors for the achiral equilibrium configuration at $\varphi = 0.7271607\pi$, $h/\rho = 0.584$ and $\rho = 7$ are characterized by their average velocities $\langle v_x \rangle$ (blue) and average chiral indices $\langle G_0 \rangle$ (red). The attractors are approached from different orientations of the molecule. The angle α specifying the initial orientation is enclosed by the y axis and the molecule's symmetry plane containing the short molecular edge as exemplified in the panel (b) which presents a view with the z -axis perpendicular to the plane of projection. For $\alpha = 0$ the y - z -plane coincides with this symmetry plane of the molecule.

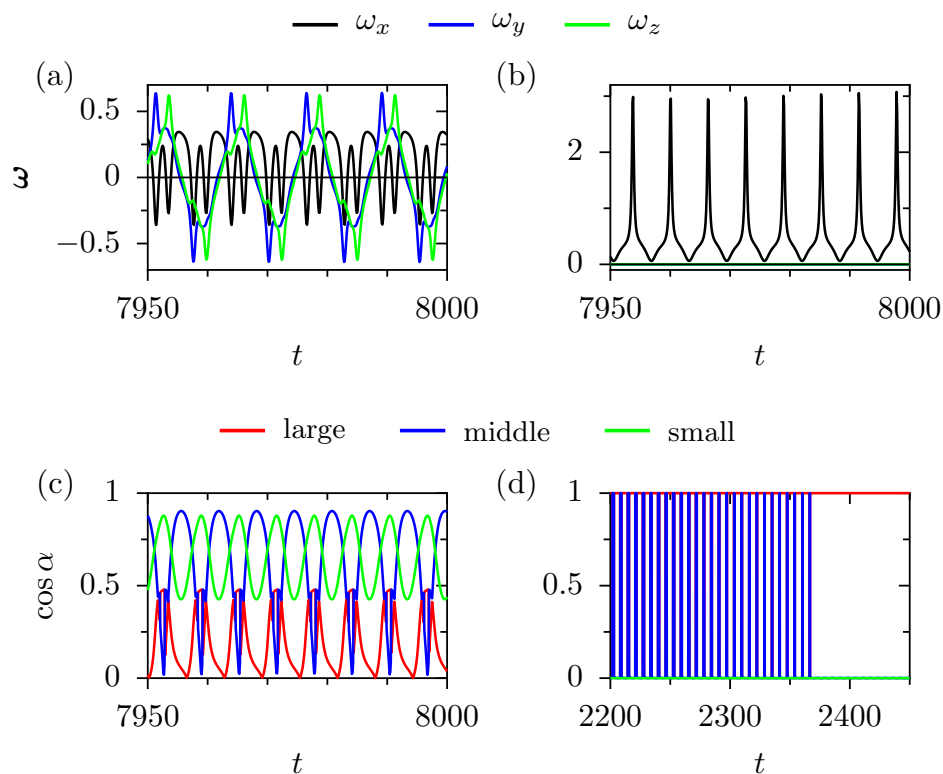


Figure 12. Different modes of the rotational motion of a molecule with $\varphi = 0.7271607\pi$, $h/\rho = 0.584$ and $\rho = 7$ corresponding to an achiral equilibrium configuration on the $(h/\rho)_1$ -curve. In the upper row the components ω_x (black), ω_y (blue), and ω_z (green) of the instantaneous rotation axis are displayed; the lower row presents the cosines of angles between the large (red), middle (blue) and small (green) principal axes and the x -axis. The left column corresponds to the asymptotic state with larger positive velocity in x -direction $\langle v_x \rangle = 0.0025$ and the right column to the asymptotic state with smaller positive velocity in x -direction, $\langle v_x \rangle = 0.000083$. In case of the large positive velocity the molecule performs a tumbling but yet periodic motion as can be seen both from the oscillatory behavior of the instantaneous rotation axis (a) and the alignment of the instantaneous axis with the x -axis (c). In the asymptotic state of slow motion the instantaneous rotation axis exactly points into the x -direction (b). Asymptotically (for times $t > 2360$) the large principal axis strictly lies in the x -direction (d). In a transient period at earlier times the molecular orientation switches between perfect x -alignments with the large and the middle principal axes (d).

the resulting averaged velocities in x -direction. The emerging pattern is essentially symmetric about $\langle v_x \rangle = 0$ and consists of different branches and a region with a cloud of apparently random points. The deviations from symmetry are insignificant within statistical uncertainty. While, on the branches, the center of mass approaches an average motion with constant velocity $\langle v_x \rangle$, superimposed by short oscillations, in the cloud region it asymptotically oscillates with a period which is larger than the width of the averaging window, see in Fig. 14. Hence, the resulting averages over a window that is shorter than a period are randomly distributed within an upper and a lower bound. The true averages extended over a full period are zero within numerical precision.

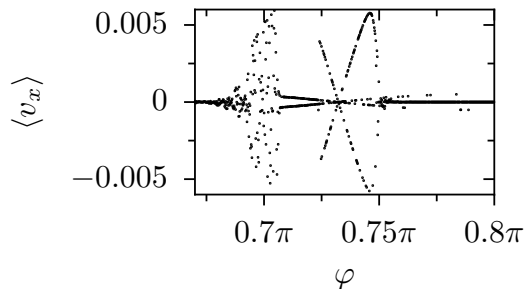


Figure 13. Average velocities in the x -direction for 2000 randomly rotated initial conditions taken along the achiral curve $(h/\rho)_1$ given by eq. (22) are displayed for $\rho = 5$ and $\varphi \in [0.67\pi, 0.8\pi]$ in steps of $\Delta\varphi = 1.65 \cdot 10^{-4} \pi$. The equations of motion (11) were numerically solved with these initial conditions up to the time $t = 8000$ and the average $\langle v_x \rangle$ was estimated by means of eq. (20) for $t_0 = 7000$, $\tau = 1$ and $N = 1000$. Apart from the region $\varphi \in (0.68\pi, 0.7066\pi)$ where the average velocities seemingly are random, they form up to four branches. Coming in pairs of opposite average velocities they maintain the achiral symmetry at each point along the achiral curve. On the part of the achiral curve with $\varphi \in [0.8\pi, \pi]$, which is not shown, the lateral average velocity forms a single branch with $\langle v_x \rangle = 0$ within numerical precision.

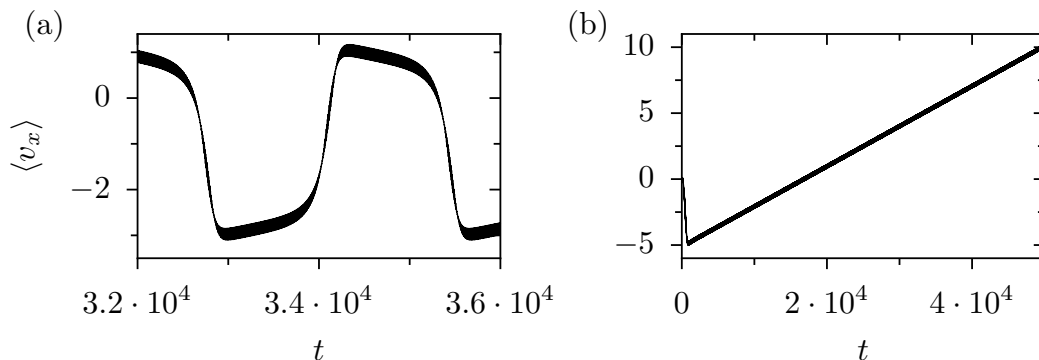


Figure 14. The center of mass motion on the achiral curve, eq. (22) (a) for $\varphi = 0.7\pi$, and (b) $\varphi = 0.71092\pi$, both for $\rho = 5$. The long period $T \approx 2730$ in (a) leads to an under-sampling of the average $\langle v_x \rangle$ displayed in Fig. 13 and as a consequence to the cloud of random points in the screw angle region between 0.66π and 0.7066π . In contrast, the case in panel (b) approaches a uniform motion in the positive x direction after a short transient.

As for the case of chiral equilibrium configurations, also for achiral equilibrium configurations the number of branches in the present investigation varies from one up to four. In the limiting cases of $\varphi = 2/3\pi$ and $\varphi = \pi$ the configurations on the achiral curve are planar and only a single branch with $\langle v_x \rangle = 0$ exists. Additional branches appear for intermediate values of φ always in pairs with positive and negative velocities and opposite chiral indices, while the zero-velocity and zero-chirality-index branch may become unstable. Branches with opposite velocities and chiral indices always occur with equal weight such that the mirror symmetry of the initial achiral configuration is restored. For $\varphi = \arccos(-2/3) \approx 0.732\pi$, corresponding to a regular tetrahedron, four

velocity branches cross each other at $\langle v_x \rangle = 0$, see Fig. 13.

The present phenomenon of dynamical symmetry breaking is different from the one that was reported in Ref. [17] where molecules with initially achiral geometric configurations, but with different bond strengths, were considered. Hence those molecules were chiral from the outset with respect to their mechanical properties. We emphasize here that the effect of dynamical symmetry breaking occurs for achiral molecules with respect to both geometry and bond strengths.

4. Role of hydrodynamic interactions

In order to clarify the role of hydrodynamic interactions for the transport of chiral objects in a shear flow, we compared the motion of a spiral molecule with screw angle $\varphi = \pi/2$, relative rise $h/\rho = 0.584$ and radius $\rho = 7$ in presence of three different vector fields describing the action of the fluid on the molecule at different levels of accuracy. In the crudest approximation the forces contribute to the velocity in terms of the Stokes law for which the mobility tensor simplifies to

$$\mathbf{H}_{i,j}^{\text{Stokes}} = \frac{1}{6\pi\eta a} \mathbb{1} \delta_{i,j} . \quad (24)$$

Leading corrections in the ratios of the atomic radius to intra-molecular distances are contained within the Oseen approximation, yielding

$$\mathbf{H}_{i,j}^{\text{Oseen}} = \mathbf{H}_{i,j}^{\text{Stokes}} + \frac{1 - \delta_{i,j}}{8\pi\eta r_{i,j}} \left[\mathbb{1} + \frac{\mathbf{r}_{i,j} \mathbf{r}_{i,j}}{r_{i,j}^2} \right] . \quad (25)$$

Finally we compared the Stokes and Oseen results with those following from the full Rotne-Prager tensor (6). Since we found only minor differences between the outcomes of the Oseen and Rotne-Prager treatment, see Fig. 5(a), we only present results of the comparison between Stokes and Rotne-Prager. It is interesting to note that the rotational motion and the internal motion of the molecule qualitatively are quite similar for the Stokes and the Rotne-Prager treatment. Fig. 15 exemplifies the qualitative agreement of the two approximations by comparing the alignment of (a) the middle principal axis with the instantaneous rotation axis and (b) the x -component of the instantaneous rotation axis.

Also the deformational motion of the molecule is quite similar, see Fig. 16 comparing the magnitudes of the principal axes and the relative volume for the two approximations. Hence the rotational and internal motion of a molecule is mainly determined by the action of the Stokes forces.

In the present case of uniform shear flow the sole action of the Stokes forces cannot lead to a translational motion in the vorticity direction. This rigorously follows from the fact that the internal molecular forces exerted by the intra-molecular FENE-Fraenkel springs do not contribute to the motion of the center of mass for a uniform shear flow within the Stokes approximation, $\sum_{i,j} \mathbf{H}_{i,j}^{\text{Stokes}} \mathbf{F}_j = 0$, and hence the center of mass

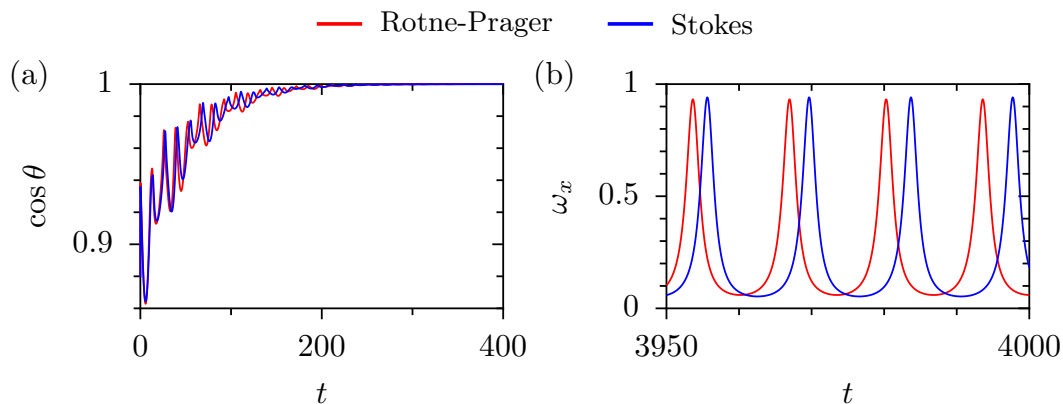


Figure 15. A comparison of the rotational motion of a molecule under the sole action of the Stokes forces (blue) and the full Rotne-Prager tensor (red) is presented for a spiral molecule with $\varphi = 0.87$, $h/\rho = 0.2073$ and $\rho = 7$ with an initial orientation that leads to the uppermost velocity branch (see Fig. 5(a)) within the Rotne-Prager treatment. The panel (a) displays the approach of the angle between the instantaneous rotation axis and the middle principal axis, showing good agreement of the Stokes and Rotne-Prager treatment. (b) The oscillations of the x -component of the instantaneous rotation axis follow the same pattern with the same amplitude and slightly smaller period under the influence of the Rotne-Prager mobility as for the Stokes forces.

motion is determined by

$$\dot{\mathbf{X}} = \sum_n \mathbf{v}(\mathbf{x}_n). \quad (26)$$

Therefore, in a uniform shear flow, as given by eq. (10), the center of mass cannot move perpendicularly to the flow direction within the Stokes approximation and the lateral drift consequently vanishes. Only the small, non-diagonal terms of the mobility tensor implied by both the Oseen and Rotne-Prager treatment lead to a coupling between the translational and the rotational motion and, in this way facilitate a center of mass motion perpendicular to the flow direction. For more complicated flow fields with non-uniform vorticity such a coupling becomes possible and may lead to chiral separation even within the Stokes approximation [1].

5. Conclusions

We presented a case study of the dynamics of deformable chiral objects consisting of four spheres in a uniform shear flow. These objects, which we have called molecules, consist of four spherical atoms. Internal forces due to relative position changes of the atoms were modeled by FENE-Fraenkel forces such that the bond lengths may only vary within a prescribed range. In the equilibrium configuration the internal forces balance each other. Forces exerted by the fluid on the molecule drive the molecule out of this equilibrium state. Due to the small size and mass of the atoms, inertia terms in the equations of motion could be neglected and a purely overdamped motion

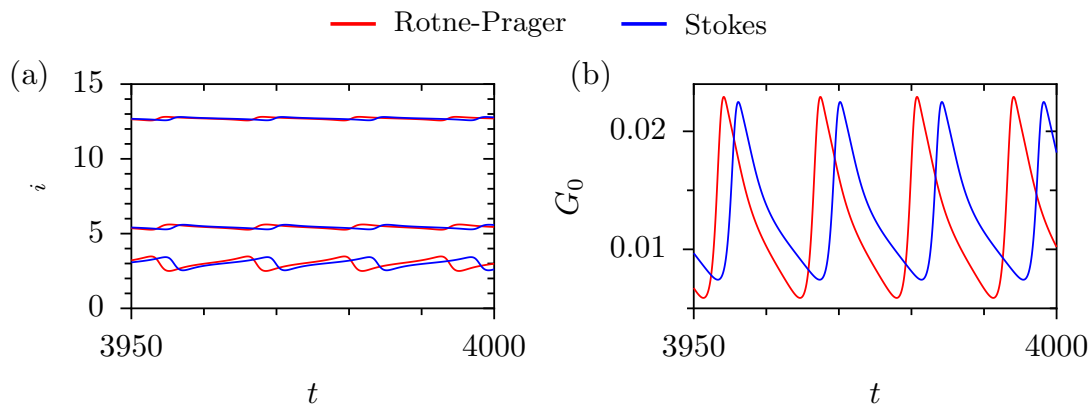


Figure 16. For the parameter values detailed in Fig. 15, the hydrodynamic interactions contained in the full Rotne-Prager mobility tensor (red) have little influence on the magnitudes of the principal axes displayed in panel (a) compared to the sole action of Stokes forces (blue). Also the chirality index presented in (b) differs in a small shift of the period, which is slightly shorter, and in the amplitude which is larger in the case of the Rotne-Prager treatment.

was studied. The influence of the flowing fluid on the molecules was described by means of the Rotne-Prager mobility tensor; this tensor includes the Stokes force and hydrodynamic interactions (up to second order in the atom radius to intra-molecular distance ratio) between the atoms of a molecule. If only the Stokes forces are considered and hydrodynamic interactions are neglected then the molecule moves in a uniform shear flow with its center of mass strictly in the direction of the flow field. Moreover it also performs a rotational motion about the center of mass with an instantaneous rotation axis pointing into the direction of vorticity. However, the hydrodynamic interactions cause a coupling between the translational and the rotational motion of the molecule. These interactions let the rotating molecule act as a propeller which drives the molecule transversely to the flow field in or against the direction of its vorticity. The direction of this component of motion is opposite for a molecule and its mirror images, thus leading to different transport properties of enantiomers.

In general, one finds different asymptotic forms of motion for molecules with the same equilibrium configuration. These motional states correspond to different attractors of the equations of motion. They can be distinguished by the magnitude of their average velocities in vorticity direction and the orientation of the molecule relative to the instantaneous rotation axis which typically points into the vorticity direction. The maximum number of attractors that we identified in the present study was four; this corresponds to (i) two alignments of the instantaneous axis of rotation with the large and the small principal axes and (ii) two alignments with the middle axis. We documented the typical translational, rotational and deformational motion in detail with the example of a molecule with a particular equilibrium configuration. The same qualitative motion patterns were observed for numerous other equilibrium configurations but not presented here.

The reason why we studied deformable molecules rather than rigid objects was not only to obtain a more realistic modeling but also because the numerical implementation of the constraints defining rigid objects in three dimensions is more difficult than allowing for deformations. Moreover we found that the flexibility of the molecules may lead to dynamical symmetry breaking for molecules with achiral equilibrium configurations. We demonstrated that the deformations of achiral molecules may lead to chiral configurations with finite chirality index G_0 accompanied by a finite average lateral velocity in or opposite to the vorticity direction. If the initial conditions are sampled from a symmetric distribution, containing mirror-symmetry related orientations with equal weight, then motional states with opposite chirality emerge with equal probability. In this way the mirror symmetry of the total state space is recovered.

The effects of chirality on the transport properties are relatively weak in the present case of a uniform shear flow. This finding is also in agreement with the results of Ref. [17] for bond-strength induced chirality. The situation though is expected to drastically change for non-uniform shear flows. It is plausible to assume that there, locally, still the same principal mechanisms are at work: The local vorticity leads to a rotation of the molecule which then acts via hydrodynamic interactions as a propeller pushing itself in or opposite to the direction of the instantaneous rotation axis depending on its chirality. In non-uniform shear flows molecules of different chirality, however, will be moved to different regions of the flow-field where they then are advected with different velocities. This effect can significantly enhance the influence of the chirality on transport properties and hence, may form the basis of an effective, purely physical enantiomer-separation mechanisms.

Before such practical applications can be envisaged, however, the so far neglected influences of thermal noise, hydrodynamic interactions between different molecules of same and different chirality as well as between molecules and walls confining the fluid should all be taken into account and investigated.

Acknowledgments

We express our sincere thanks to Marcin Kostur and Juyeon Yi for valuable discussions. This project has been supported by the Deutsche Forschungsgemeinschaft (DFG), grant number HA-1517/28-1.

Appendix A. Achiral configurations

By the construction of the spiral molecules, the length $d_{n,m}$ of the edge connecting the n th with the m th atom only depends on the absolute value of the difference between n and m , $d_{n,m} = l(|n - m|)$. In the general case, a spiral molecule hence has three equal edges of length $l(1)$, two of length $l(2)$ and one of length $l(3)$ where

$$l(n) = [2\rho^2(1 - \cos(n\varphi)) + n^2h^2]^{1/2}. \quad (\text{A.1})$$

One branch of achiral configurations possesses two equilateral and two isosceles faces, see Fig 3(c). They have five equally long edges with $l(1) = l(2)$. This condition determines the relative rise as a function of the screw angle to read

$$(h/\rho)_1^2 = \frac{2}{3}(\cos(2\varphi) - \cos(\varphi)) , \quad (\text{A.2})$$

where the screw angle is restricted to $2\pi/3 < \varphi < 4\pi/3$ in order that the right hand side stays positive. On this curve the maximal value of the relative rise is reached at $\varphi = \pi$ and there takes the value $h/\rho = 2/\sqrt{3}$.

Achiral configurations with four identical isosceles faces result from the requirement $l(1) = l(3)$. The relative rise as a function of the screw angle then becomes

$$(h/\rho)_2^2 = \frac{1}{4}(\cos(3\varphi) - \cos(\varphi)) , \quad (\text{A.3})$$

with $\pi/2 < \varphi < 3\pi/2$. This function vanishes at $\varphi = \pi$ as well as at the borders of the indicated interval, and has a maximum at $\varphi \approx 0.696\pi$, $h/\rho \approx 0.620$.

The two achiral branches cross at the special angle at which $\cos \varphi = -2/3$ yielding $h/\rho = \sqrt{10/27}$, where all three edge lengths agree with the each other, resulting in a regular tetrahedron.

References

- [1] Kostur M, Schindler M, Talkner P and Hänggi P 2006 *Phys. Rev. Lett.* **96** 014502
- [2] Hänggi P and Marchesoni F 2009 *Rev. Mod. Phys.* **81** 387
- [3] Crusats J, El-Hachemi Z and Ribó JM 2010 *Chem. Soc. Rev.* **39** 569
- [4] Howard DW, Lightfoot EN and Hirschfelder JO 1976 *AIChE Journal* **22** 794
- [5] de Gennes PG 1999 *Europhys. Lett.* **46** 827
- [6] Brenner H 1964 *Chem. Eng. Sci.* **19** 631
- [7] Chen P and Chao CH 2007 *Phys. Fluids* **19** 017108
- [8] Makino M, Arai L and Doi M 2008 *J. Phys. Soc. Japan* **77** 064404
- [9] Marcos, Fu HC, Powers TR and Stocker R 2009 *Phys. Rev. Lett.* **102** 158103
- [10] Grzybowski BA and Whitesides GM 2002 *Science* **296** 718
- [11] Ghosh A and Fischer P 2009 *Nano Lett.* **9** 2243
- [12] D'Urso, A Randazzo R, Lo Faro L and Purrello R 2010 *Angew. Chem. Int. Ed.* **49** 108
- [13] Doi M and Makino M 2005 *Phys. Fluids* **17** 043601
- [14] Makino M and Doi M 2005 *Phys. Fluids* **17** 103605
- [15] Eichhorn R 2010 *Phys. Rev. Lett.* **105** 034502
- [16] Eichhorn R 2010 *Chem. Phys.* **375** 568
- [17] Watari N and Larson RG 2009 *Phys. Rev. Lett.* **102** 246001
- [18] Hsieh CC, Jain S and Larson RG 2006 *J. Chem. Phys.* **124** 044911
- [19] Purcell EM 1977 *Am. J. Phys.* **45** 3
- [20] Rotne J and Prager S 1969 *J. Chem. Phys.* **50** 4831
- [21] Dhont JKG 1996 *An Introduction to Dynamics of Colloids* (Amsterdam: Elsevier)
- [22] Radhakrishnan K and Hindmarsh AC 1993 LLNL report UCRL-ID-113855
- [23] Petzold L 1983 *SIAM J. Sci. Stat. Comput.* **4** 136
- [24] Jones E, Oliphant T, Peterson P *et al* 2001 *SciPy: Open source scientific tools for Python* (<http://www.scipy.org/>)
- [25] Solymosi M, Low RJ, Grayson M and Neal MP 2002 *J. Chem. Phys.* **116** 9875
- [26] Harris AB, Kamien RD and Lubensky TC 1999 *Rev. Mod. Phys.* **71** 1745

- [27] In order to draw elements out of the Haar measure of $SO(3)$ we first generate a random vector with three independent Gaussian components about which a rotation with an angle α is performed. To guarantee a uniform coverage of the rotation group, the rotation angle $\alpha \in [0, \pi]$ must be drawn from the probability density $(1/\pi) \sin^2(\alpha/2)$, [28].
- [28] Miles RE 1965 *Biometrika* **52** 636
- [29] Reimann P and Hänggi P 2002 *Appl. Phys. A* **75** 169